NASA-CR-195703



Department of Aerospace Engineering
University of Maryland
College Park, Maryland 20742

# A Parametric Sensitivity Study for Single-Stage-to-Orbit Hypersonic Vehicles Using Trajectory Optimization

T. Alan Lovell and D. K. Schmidt
Dept. of Aerospace Engineering
University of Maryland
College Park, Maryland

prepared for

NASA Langley Research Center

under Grant No. NAG1-1540

Ms. Irene Gregory, Technical Monitor

Interim Tech Report

March 21, 1994

## TABLE OF CONTENTS

## ABSTRACT

The class of hypersonic vehicle configurations with single stage-to-orbit (SSTO) capability reflect highly integrated airframe and propulsion systems. These designs are also known to exhibit a large degree of interaction between the airframe and engine dynamics. Consequently, even simplified hypersonic models are characterized by tightly coupled nonlinear equations of motion. In addition, hypersonic SSTO vehicles present a major system design challenge: The vehicle's overall mission performance is a function of its subsystem efficiencies, including structural, aerodynamic, propulsive, and operational. Further, all subsystem efficiencies are interrelated, hence, independent optimization of the subsystems is not likely to lead to an optimum design. Thus, it is desired to know the effect of various subsystem efficiencies on overall mission performance. For the purposes of this analysis, mission performance will be measured in terms of the payload weight inserted into orbit. In this report, a trajectory optimization problem is formulated for a generic hypersonic lifting body for a specified orbit-injection mission. A solution method is outlined, and results are detailed for the generic vehicle, referred to as the baseline model. After evaluating the performance of the baseline model, a sensitivity study is presented to determine the effect of various subsystem efficiencies on mission performance. This consists of performing a parametric analysis of the basic design parameters, generating a matrix of configurations, and determining the mission performance of each configuration. Also, the performance loss due to constraining the total head load experienced by the vehicle is evaluated. The key results from this analysis include the formulation of the sizing problem for this vehicle class using trajectory optimization, characteristics of the optimal trajectories, and the subsystem design sensitivities.

## NOMENCLATURE

| | |
|---|---|
| $a$ | sonic velocity |
| $A_e$ | engine exit area |
| $A_N$ | engine nozzle area ratio |
| $C_D$ | vehicle drag coefficient |
| $C_{Do}$ | profile drag coefficient |
| $C_L$ | vehicle lift coefficient |
| $C_p$ | specific heat at constant pressure for air |
| $D$ | vehicle drag |
| $E$ | vehicle energy height |
| $g$ | gravitational constant |
| $h$ | vehicle altitude above Earth's surface |
| $k$ | ratio of specific heats |
| $L$ | vehicle lift |
| $L_n$ | vehicle forebody length |
| $M_\infty$ | freestream Mach No. |
| $M_2$ | diffuser exit Mach No. |
| $M_3$ | combustor exit Mach No. |
| $M_e$ | engine exit Mach No. |
| $p_\infty$ | freestream pressure |
| $p_s$ | surface pressure on vehicle forebody |
| $q_\infty$ | freestream dynamic pressure |
| $Q$ | vehicle heat load |
| $R$ | vehicle distance from Earth's center |
| $R_e$ | radius of Earth |
| $S$ | effective frontal area |
| $T$ | engine thrust |
| $V$ | vehicle velocity |
| $W$ | total vehicle weight |
| $W_e$ | effective vehicle width |
| $\dot{W}_f$ | vehicle fuel flow rate |
| $\alpha$ | vehicle angle of attack |
| $\alpha_n$ | forebody nose angle |
| $\gamma$ | vehicle flight path angle |
| $\rho_\infty$ | freestream density |
| $\omega_e$ | Earth's rate of rotation |

# I. INTRODUCTION

A possible next-generation launch vehicle will be a fully reusable, single-stage-to-orbit, manned aerospacecraft. Such vehicles will most likely use liquid hydrogen fuel, be 100 to 150 feet in length, and weigh approximately 300,000 lbs [1]. They should be capable of horizontal take-off and landing, accelerating to Mach 25 on orbit, as well as cruising at Mach 5 to 15 in the upper atmosphere.

In order to meet the above stated mission requirements, the vehicle must utilize an airbreathing propulsion system for much of its trajectory, to avoid the weight penalty of carrying the oxidizer on board. The untested SCRAMjet engine will likely be the primary propulsive system. To obtain maximum propulsive efficiency, the SCRAMjet engine must be operated at a high dynamic pressure. However, since aerodynamic heating and drag also increase with dynamic pressure, the benefits of high propulsive efficiency must be balanced against temperature and structural constraints. Further, propulsive variables such as thrust and fuel flow vary with Mach number and altitude, so propulsive efficiency will depend on the vehicle trajectory. Similarly, both aerodynamic forces and heating are functions of Mach number and altitude, thus aerodynamic efficiency and structural design requirements (e.g., the amount of aerodynamic heating the structure can withstand) are trajectory-dependent as well. This demonstrates the highly interactive nature of these systems. As such, it should be reiterated that independent subsystem optimization will not lead to the optimal integrated system.

Since these vehicles are neither conventional aircraft nor rocket, the vehicle sizing problem is unique. Conventional aircraft sizing, based on Breguet analysis for example, is not appropriate, nor is classic rocket performance analysis. Consequently, the sizing problem must be reformulated. A new formulation and some parametric results are presented in this paper. First, a baseline hypersonic vehicle configuration is defined. Also defined are several high-efficiency configurations, each resulting from a change in the efficiency of one of the vehicle's many subsystems. A minimum-fuel optimization problem for these configurations is then posed. After a numerical solution algorithm is outlined, the resulting characteristics of the baseline trajectory are detailed. Also, the effect of constraining the total heating load experienced by the vehicle during the mission will be assessed. Finally, a parametric analysis will be performed to determine the sensitivities between mission performance and subsystem efficiencies.

## II. DESCRIPTION OF BASELINE VEHICLE AND ATMOSPHERIC MODEL

The vehicle geometry considered in this study is generic, but was selected to reflect key characteristics similar to the X-30 vehicle described in [1]. Figure 1 shows a simplified sketch of the baseline vehicle. The basic aerodynamic and propulsive modeling of the vehicle has been addressed in [4] and [5]. The configuration consists of a forebody/engine inlet, internal engine module, and afterbody/exhaust nozzle.

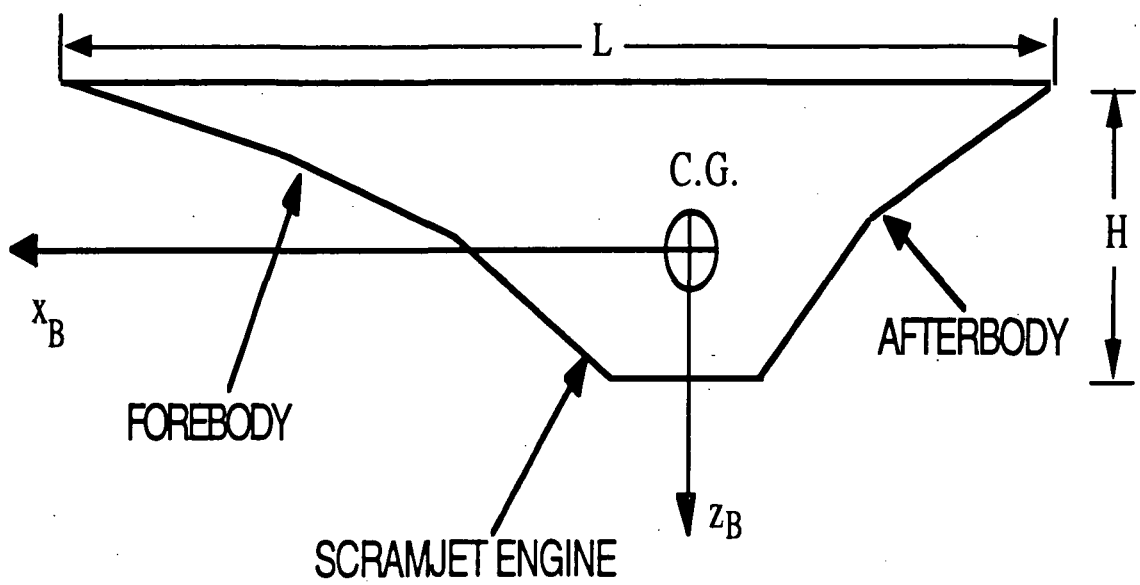


Fig. 1. Hypersonic Vehicle Configuration.

### 2.1 Aerodynamic Characteristics

The forebody, with forebody nose angle $\alpha_n$, is the primary lifting surface. If the vehicle angle of attack is $\alpha$, under Newtonian theory the pressure on the forebody is

$$p_s = p_\infty + q_\infty(1-\cos 2(\alpha + \alpha_n)) \qquad (2.1.1)$$

If the pressure on the upper surface is assumed constant at $p_\infty$, the resulting lift and drag on the forebody are

$$L = L_n W_e \cos(\alpha + \alpha_n) q_\infty (1 - \cos 2(\alpha + \alpha_n)) \quad (2.1.2)$$

$$D = L_n W_e (\sin(\alpha + \alpha_n)\, q_\infty (1 - \cos 2(\alpha + \alpha_n)) + q_\infty C_{D_o}) \quad (2.1.3)$$

These equations can be arranged as

$$L = q_\infty S C_L \quad (2.1.4)$$

$$D = q_\infty S C_D \quad (2.1.5)$$

where

$$S = L_n W_e \quad (2.1.6)$$

$$C_L = (1 - \cos(2(\alpha + \alpha_n)))\cos(\alpha + \alpha_n) \quad (2.1.7)$$

$$C_D = C_{D_o} + (1 - \cos(2(\alpha + \alpha_n)))\sin(\alpha + \alpha_n) \quad (2.1.8)$$

For this model, a constant $C_{D_o}$ of .024 has been chosen [6]. Figure 2 shows the aerodynamic drag polar.

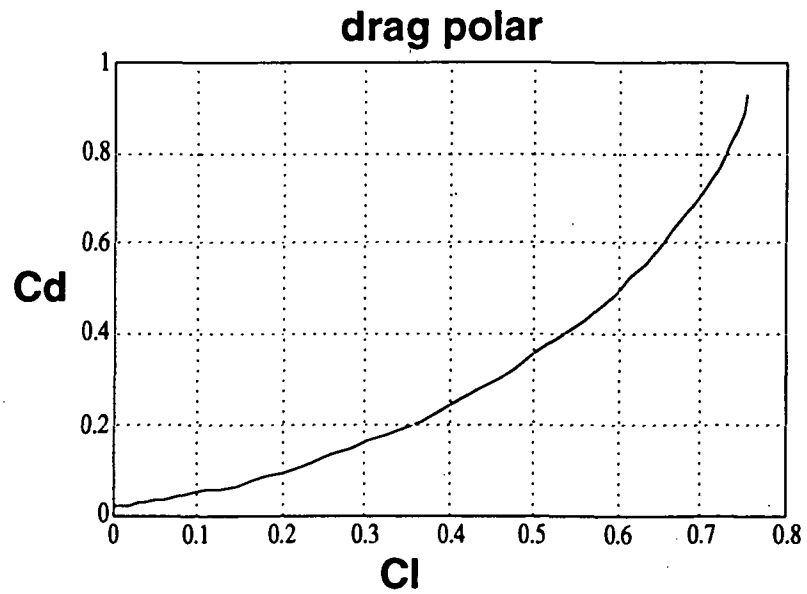


Fig. 2. Vehicle Drag Polar.

## 2.2 Propulsive Characteristics

The SCRAMjet engine modeling is presented in [4], [5], and [7]. The thrust and fuel flow characteristics of the baseline engine module are

$$\text{Thrust} / (p_\infty A_e) = C_1 F^{(k/(k-1))} - C_2 (k M_\infty^2 + 1) / [M_\infty F^{(k+1)/(2(k-1))}] \quad (2.2.1)$$

$$\text{Fuel flow} / (p_\infty A_e a) = C_3 F^{(3k-1)/(2(k-1))} \quad (2.2.2)$$

where

$$k = 1.4 \quad (2.2.3)$$

$$F = 1 + ((k+1)M_\infty^2)/2 \quad (2.2.4)$$

$$A_e = A_{e_0} \exp(-C_4(M_\infty - 1)) \quad (2.2.5)$$

$$A_{e_0} = 840 \text{ ft}^2 \quad (2.2.6)$$

$$a = 1000 \text{ ft/sec} \quad (2.2.7)$$

Note that $A_e$ is assumed to be a function of Mach number, which reflects the fact that the number of engine modules operating may be a Mach-dependent variable. The function (2.2.5) is itself a curve-fit of empirical data, with $C_4$ taking on a value of approximately .2.

For this analysis, the engine quantities have been calculated assuming fixed chosen values for combustor exit Mach number, nozzle area ratio, and heat input to the combustor. The engine dependent constants $C_1$ through $C_3$ are defined below as

$$c_1 = \left[\frac{(k M_e^2 + 1)(k M_2^2 + 1)}{(k M_3^2 + 1)}\right]\left[\frac{\left(1 + \frac{k-1}{2} M_3^2\right)}{\left(1 + \frac{k-1}{2} M_e^2\right)\left(1 + \frac{k-1}{2} M_2^2\right)}\right]^{\frac{k}{k-1}} \quad (2.2.8)$$

$$c_2 = \frac{M_2}{A_N \sqrt{\left(1 + \frac{k-1}{2} M_2^2\right)^{\frac{k+1}{k-1}}}} \quad (2.2.9)$$

$$c_3 = \frac{Cp}{RQ} \frac{M_2}{A_N \sqrt{\left(1 + \frac{k-1}{2} M_2^2\right)^{\frac{k+1}{k-1}}}} \left[ \left(\frac{M_3}{M_2}\right)^2 \left(\frac{1 + \frac{k-1}{2} M_3^2}{1 + \frac{k-1}{2} M_2^2}\right) \left(\frac{k M_2^2 + 1}{k M_3^2 + 1}\right)^2 - 1 \right] \qquad (2.2.10)$$

where Q and R in (3.2.9) represent heating value of the fuel and gas constant for air, respectively. All of the quantities in (3.2.7)-(3.2.9) are taken to be constant for a specific engine configuration. Therefore, the three engine constants will remain fixed over the trajectory. The values of the engine constants taken for this analysis are

$$C_1 = 0.1 \qquad (2.2.11)$$

$$C_2 = 0.03 \qquad (2.2.12)$$

$$C_3 = 8 \times 10^{-10}/\text{ft} \qquad (2.2.13)$$

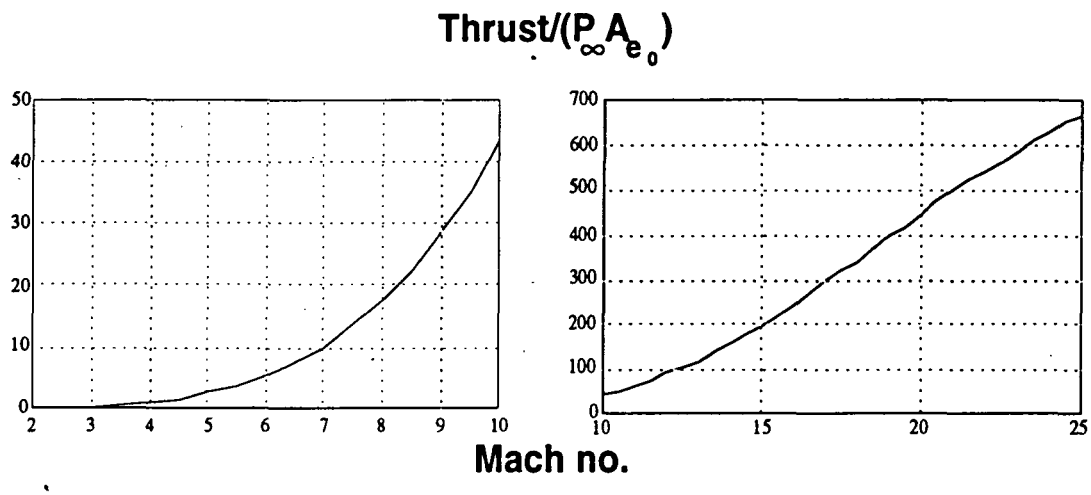


Fig. 3. Variation of Thrust with Mach number.

The variation of thrust with Mach number is plotted in Figure 3. Note that this is a plot of Eqn (3.2.1) above multiplied by $A_e/A_{e_o}$, thus allowing for the Mach-dependent area. Figure 4 shows specific fuel consumption vs. Mach number. Although thrust (lb) and fuel flow rate (lb/hr) are functions of Mach number and altitude, Figures 3 and 4 vary with *Mach number only*.

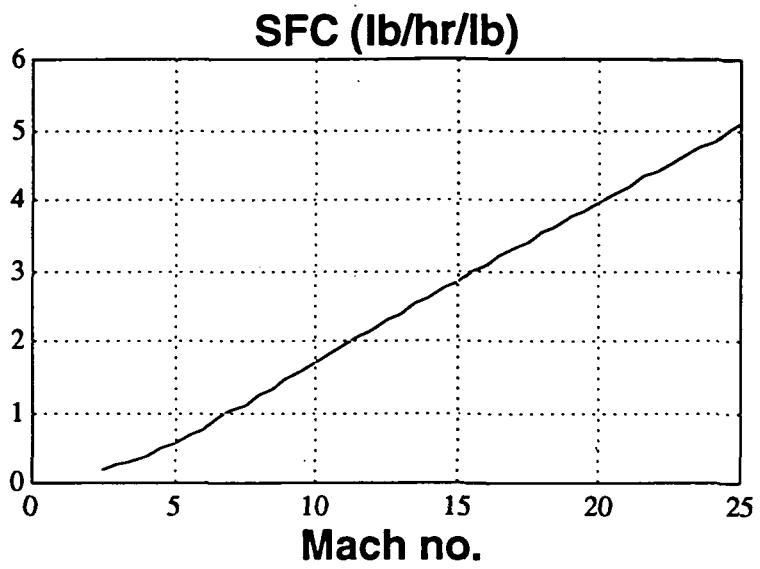


Fig. 4. Variation of S.F.C. with Mach number.

## 2.3 Atmospheric Model

For the trajectory study deiscussed later in this report, a simplified exponential atmosphere was used, resulting in the following model for freestream pressure $p_\infty$ and density $\rho_\infty$:

$$p_\infty = p_{ref} \exp\left[\frac{-g}{R_{gas} T_{ref}} (h - h_{ref})\right] \tag{2.3.1}$$

$$\rho_\infty = \rho_{ref} \exp\left[\frac{-g}{R_{gas} T_{ref}} (h - h_{ref})\right] \tag{2.3.2}$$

where h is altitude and

$$h_{ref} = 150{,}000\text{ft} \tag{2.3.3}$$

$$p_{ref} = 2.51\text{ psf} \tag{2.3.4}$$

$$\rho_{ref} = 2.87 \times 10^{-6}\text{ sl/ft}^3 \tag{2.3.5}$$

$$\frac{-g}{R_{gas} T_{ref}} = 3.68 \times 10^{-5}\text{/ft} \tag{2.3.6}$$

## III. PARAMETRIC CONFIGURATION MATRIX

Having set forth the characteristics of the baseline configuration, it can now be determined how to model an increase in the efficiency of the configuration's various subsystems in order to determine the effect of each increase on mission performance. As stated earlier, mission performance is measured in terms of the amount of payload inserted into orbit, i.e., the vehicle's orbital mass fraction. The orbital mass fraction is the sum of the structural and payload mass fractions:

$$W_{final}/W_{initial} = (W_{payload} / W_{initial}) + (W_{structure} / W_{initial})$$

So for a given orbital mass fraction, structural mass fraction trades one to one with payload mass fraction. Finally, the operational efficiency is maximized if the trajectory leads to the maximum orbital mass fraction.

The initial and final energy levels of the vehicle's trajectory are to be specified (and hence known). Thus, by expressing energy as a function of mass fraction, the effects of the subsystem efficiencies on orbital mass fraction can be examined. Consider a simplified form of the energy equation as follows:

$$\frac{dE}{dt} = \frac{V}{W}(T-D) \tag{3.1}$$

$$\left(\frac{dE}{dW}\right)\left(\frac{dW}{dt}\right) = T\left(\frac{V}{W}\right)\left(1-\frac{D}{T}\right) \tag{3.2}$$

$$\frac{dE}{dW}\left(-\dot{W}_f\right) = T\left(\frac{V}{W}\right)\left[1-\left(\frac{D}{T}\right)\left(\frac{W}{L}\right)\right] \quad \text{(assuming L = W)} \tag{3.3}$$

$$dE = V\left(\frac{T}{\dot{W}_f}\right)\left[\left(\frac{D}{T}\right)\left(\frac{W}{L}\right)-1\right]\frac{dW}{W} = \frac{V}{s.f.c.}\left[\frac{1}{\left(\frac{L}{D}\right)}\frac{1}{\left(\frac{T}{W}\right)}-1\right]\frac{dW}{W}$$

or, since $dW_f = -dW$,

$$\frac{dE}{dW_f} = \frac{V}{W\,(s.f.c.)}\left[1-\frac{1}{\left(\frac{L}{D}\right)}\frac{1}{\left(\frac{T}{W}\right)}\right] \tag{3.4}$$

Equation (3.4) reveals the overall system efficiency, or the energy gain per unit of fuel used. In this relation one observes that the s.f.c., the thrust-to-weight ratio, and the lift-to-

drag ratio are significant, along with the flight velocity. Obviously, the greater the system efficiency for a given mission, the greater the orbital mass fraction $W_{final}/W_{initial}$.

The mission performance is therefore a function of the following subsystem efficiencies:

(L/D) - Aerodynamic Efficiency

(T/W) and s.f.c. - Propulsive Efficiencies

In addition to the baseline vehicle configuration, three other vehicle configurations are generated: one representing an increase in aerodynamic efficiency, and two representing increases in propulsive efficiency. These configurations will be labeled as the high-(L/D), high-(T/W), and low-s.f.c. configurations. For each configuration, one of the subsystem efficiency parameters is increased while the other two are kept at their baseline values. Table 1 presents a configuration matrix indicating the efficiency values for each configuration considered. All efficiency parameters are evaluated at the nominal initial condition: The baseline L/D in Table 1 is defined by evaluating the lift and drag equations for the baseline vehicle at $\alpha = 0$, while T/W and s.f.c. are evaluated at the initial Mach number of 2.5. Increases in each of the subsystem efficiencies are modeled as follows. For the high-(L/D) model, the efficiency parameters are evaluated at the same initial condition, but with the profile drag coefficient $C_{D_0}$ set to zero. Similarly, for the low-s.f.c. configuration, the engine constant $C_3$ for the fuel flow rate was decreased by 10%. Finally, the high-(T/W) configuration was obtained by increasing $C_1$ and $C_2$ by 10% while also increasing $C_3$ by 10% to maintain the same s.f.c. as the baseline vehicle.

**Table 1 - Comparison of Baseline Configuration With Three Improved Subsystem Efficiency Models**

| Model | $(L/D)_o$ | $(T/W)_o$ | $(SFC)_o$ (lb/hr/lb) |
|---|---|---|---|
| **Baseline** | **2.206** | **.472** | **.196** |
| **High L/D** | **3.732** | **.472** | **.196** |
| **High T/W** | **2.206** | **.519** | **.196** |
| **Low SFC** | **2.206** | **.472** | **.177** |

As the table shows, increases in the subsystem efficiencies are as follows:

high-(L/D): 69% increase in $(L/D)_o$ above baseline value
high-(T/W): 10% increase in $(T/W)_o$ above baseline value
low-s.f.c.: 10% decrease in $(s.f.c.)_o$ below baseline value

As expected, each configuration shows an increase in one subsystem efficiency parameter and no change in the other two.

# IV. FORMULATION OF THE TRAJECTORY OPTIMIZATION PROBLEM

## 4.1 Optimization Paradigm

The optimization problem is formulated as follows. A baseline configuration is selected, described in terms of what will be taken as "nominal" aerodynamic and propulsive subsystem efficiencies. The question is then, for this baseline system, what is the maximum weight, or orbital mass fraction, that can be placed in orbit? This question may be answered by solving for the minimum-fuel trajectory, which leads to the maximum orbital mass fraction and the trajectory yielding maximum operational efficiency for the baseline vehicle. In addition, a heating constraint on the vehicle can be imposed. The initial solution desired is that for unconstrained heating (i.e., the maximum orbital mass fraction that can be obtained without regard to heat load). Afterward, solutions for various specified values of maximum heat load can be obtained and compared to the nominal solution. The development below parallels that of [2].

## 4.2 Equations of Motion

The single-stage-to-orbit mission is said to be accomplished if the vehicle can transfer from an initial energy level to an orbital energy level with non-negative final weight. Here energy is measured in terms of the energy height, which is the total vehicle energy (kinetic plus potential) per unit weight. The vehicle is treated as a point mass and its motion for this analysis is constrained to be planar. The equations of motion below are for a spherical rotating earth and are relative to a coordinate frame fixed to the earth's surface [3]:

$$\dot{E} = \frac{V}{W}( T \cos \alpha - D) + \frac{V}{g} R \sin \gamma \, \omega_e^2 \qquad (4.2.1)$$

$$\dot{h} = V \sin \gamma \qquad (4.2.2)$$

$$\dot{\gamma} = \frac{g}{WV}[( L + T \sin \alpha ) - W \cos \gamma] + \left[\frac{V^2 + (R \, \omega_e)^2}{RV}\right] \cos \gamma + 2 \, \omega_e \qquad (4.2.3)$$

$$\dot{W} = -\dot{W}_f \qquad (4.2.4)$$

The energy height, E, and the altitude above the earth center, R, are defined as

$$E = h + \frac{V^2}{2g} \tag{4.2.5}$$

$$R = R_{earth} + h \tag{4.2.6}$$

The initial and final conditions are:

$h(t_0) = h_0$
$M(t_0) = 2.5$
$\gamma(t_0) = 0$
$W(t_0) = 300{,}000$ lb

(4.2.7-4.2.10)

$h(t_f) = h_f$
$M(t_f) = M_f$

(4.2.11-4.2.12)

For orbit injection, the desired values of $h_f$ and $M_f$ will be 200,000 ft and 25, respectively. The heat-transfer rate near the stagnation region as given in [8] is

$$\dot{Q} = 865\, R_n^{-1/2}(V/10^4)^{k1}(\rho/\rho_0)^{k2} \quad BTU/ft^2/sec \tag{4.2.13}$$

where $R_n$ is the vehicle nose radius. For the baseline vehicle, the above equation becomes

$$\dot{Q} = C\, \rho^{k2}\, V^{k1} \tag{4.2.14}$$

where C is a geometry-dependent proportionality constant, and $k_1$ and $k_2$ are taken to be 2.65 and 0.5, respectively. Thus the fifth equation of motion is

$$\dot{\overline{Q}} = \frac{\dot{Q}}{C} = \rho^{1/2} V^{2.65} \tag{4.2.15}$$

with boundary conditions $\overline{Q}(t_0) = 0$, and $\overline{Q}(t_f) = C_Q$. The parameter $C_Q$ is therefore proportional to the total heat load experienced by the vehicle over the trajectory. By selecting $C_Q$, the total heat load may be constrained. The following values will be used for the known constants in the equations of motion:

$$R_e = 4.8 \times 10^7 \text{ ft} \tag{4.2.16}$$

$$g = 32.2 \text{ ft}^2/\text{sec} \tag{4.2.17}$$

$$\omega_e = 2\pi \text{ rad/day} = 7.3 \times 10^{-5} \text{rad/sec} \tag{4.2.18}$$

The state vector for the model is then [E h $\gamma$ w $\bar{Q}$]. For this model, the engine is assumed to be always operating at maximum thrust, so the single control is angle of attack.

## 4.3 Nondimensionalization

Before formally setting up the problem, the variables associated with the equations of motion (except $\gamma$ and $\alpha$) are to be normalized with respect to reference quantities. The resulting nondimensional variables are:

$$\bar{E} = E/E_{ref} \qquad \bar{V} = V/V_{ref}$$

$$\bar{h} = h/h_{ref} \qquad \bar{R} = R/R_e$$

$$\bar{W} = W/W_o \qquad \bar{T} = T/(p_{ref} A_{eo})$$

$$\bar{\dot{Q}} = \dot{Q} / (\rho_{ref}^{1/2} V_{ref}^{2.65}) \qquad \bar{L} = L/(\rho_{ref} V_{ref}^2 L_n W_e)$$

$$\bar{p} = p/p_{ref} \qquad \bar{D} = D/(\rho_{ref} V_{ref}^2 L_n W_e)$$

$$\bar{\rho} = \rho/\rho_{ref} \qquad \bar{\dot{W}}_f = \dot{W}_f/(C_3\, p_{ref}\, a\, A_{eo})$$

(4.3.1-4.3.6) (4.3.7-4.3.12)

where

$$V_{ref} = 20{,}000 \text{ ft/sec}$$

$$E_{ref} = h_{ref} + .5*(V_{ref})^2 / g$$

$$W_o = 300{,}000 \text{ lb}$$

$$h_{ref} = 150{,}000 \text{ft}$$

$$p_{ref} = 2.51 \text{ psf}$$

$$\rho_{ref} = 2.87 \times 10^{-6} \text{ sl/ft}^3$$

$$A_{eo} = 840 \text{ ft}^2$$

$$a = 1000 \text{ ft/sec}$$

$$C_3 = 8 \times 10^{-10}/\text{ft}$$

(4.3.13-4.3.21)

Thus the equations of motion in nondimensional form are:

$$\dot{\bar{E}} = \frac{V_{ref}}{E_{ref}}\left[\frac{\bar{V}}{\bar{W}}\left(\frac{p_{ref}A_{eo}}{W_o}\bar{T}\cos\alpha - \frac{p_{ref}V_{ref}^2L_nW_e}{W_o}\bar{D}\right) + \frac{\bar{V}}{g}\bar{R}R_e\sin\gamma\,\omega_e^2\right] \qquad (4.3.22)$$

$$\dot{\bar{h}} = \frac{V_{ref}}{h_{ref}}\bar{V}\sin\gamma \qquad (4.3.23)$$

$$\dot{\gamma} = \frac{1}{V_{ref}}\left\{\frac{g}{\bar{V}\bar{W}}\left[\frac{p_{ref}V_{ref}^2L_nW_e}{W_o}\bar{L} + \frac{p_{ref}A_{eo}}{W_o}\bar{T}\sin\alpha - \bar{W}\cos\gamma\right] + \frac{1}{R_{ref}}\left[\frac{V_{ref}^2\bar{V}^2 + (\omega_eR_e)^2\bar{R}^2}{\bar{R}\bar{V}}\right] + 2V_{ref}\omega_e\right\} \qquad (4.3.24)$$

$$\dot{\bar{W}} = \frac{-C_3\,a\,p_{ref}\,A_{eo}}{W_o}\exp\left[\frac{-g\,h_{ref}}{R_{gas}\,T_{ref}}(\bar{h} - 1)\right]\exp\left[-.2235\left(\frac{V_{ref}\bar{V}}{a} - 1\right)\right]\left[1 + .2\left(\frac{V_{ref}\bar{V}}{a}\right)^2\right]^4 \qquad (4.3.25)$$

$$\dot{\bar{\bar{Q}}} = \bar{\rho}^{1/2}\bar{V}^{2.65} \qquad (4.3.26)$$

The initial and final conditions are:

$$\bar{h}(t_o) = \overline{h_o} \qquad \bar{h}(t_f) = \overline{h_f}$$
$$\bar{V}(t_o) = .125 \qquad \bar{V}(t_f) = \overline{V_f}$$
$$\gamma(t_o) = 0$$
$$\bar{W}(t_o) = 1$$
$$\bar{\bar{Q}}(t_o) = 0 \qquad \bar{\bar{Q}}(t_f) = \overline{C_Q}$$

(4.3.27-4.3.31) (4.3.32-4.3.34)

where $\overline{h_o} = 0$, $\overline{h_f} = 1.333$, $\overline{V_f} = 1.25$, and $\overline{C_Q} = C_Q/(\rho_{ref}^{1/2}V_{ref}^{2.65})$. Also, $\overline{E_o} = E_o/E_{ref}$ and $\overline{E_f} = E_f/E_{ref}$. For the next several sections, all variables will be referred to without the bar notation. (This includes $\bar{\bar{Q}}$, which has been normalized twice, in (2.2.15) and (2.3.4).) Hence all quantities will be assumed to be nondimensional unless otherwise specified.

## 4.4 Performance Index

The optimal trajectory will be that which requires the minimum fuel in order to ascend from an initial altitude and velocity (or energy height) to the final altitude and velocity in an unspecified time. Consequently, the performance index can be stated as

$$\min \mathbf{J} = \int_{t_0}^{t_f} \dot{W}_f \, dt \tag{4.4.1}$$

Formulation of the problem is simplified, however, if we note that minimizing fuel is equivalent to maximizing final vehicle weight, $W(t_f)$. Thus the performance index can be restated as

$$\min \mathbf{J} = -W(t_f) \tag{4.4.2}$$

This effectively changes the formulation from a Problem of Bolza to a Problem of Mayer.

4.5 Two-Point Boundary Value Problem

The problem as now defined is to minimize the above performance index subject to the above equations of motion and the specified initial and final conditions. This is a two-point boundary value problem, i.e., not all of the states and adjoints are known at either the initial time or final time. Now define the augmented performance index as

$$\min \mathbf{J} = G + \int_{t_0}^{t_f} F \, dt = -w(t_f) + \nu^T \Psi + \int_{t_0}^{t_f} \lambda^T (\mathbf{f} - \dot{\mathbf{x}}) \, dt \tag{4.5.1}$$

where

$$\Psi = [E(t_o)-E_o,\ h(t_o)-h_o,\ \gamma(t_o)-0,\ W(t_o)-1,\ Q(t_o)-0,\ E(t_f)-E_f,\ h(t_f)-h_f,\ Q(t_f)-C_Q]^T \tag{4.5.2}$$

$$\lambda = [\lambda_E\ \lambda_h\ \lambda g\ \lambda_W\ \lambda_Q]^T \tag{4.5.3}$$

$$\mathbf{x} = [E\ h\ g\ W\ Q]^T \tag{4.5.4}$$

$$\mathbf{f} = [f_1\ f_2\ f_3\ f_4\ f_5]^T \tag{4.5.5}$$

Note that $\Psi$ is simply a vector of the differences between the actual and specified initial and final conditions placed on the states. The functions $f_1$ through $f_5$ are the right-hand sides of the equations of motion in the order that they were given above. Also, define the Hamiltonian $H = \lambda^T \mathbf{f}$. The Euler-LaGrange equations--consisting of adjoint equations and control equations--can now be derived. The adjoint equations are

$$\dot{\lambda}^T = -\partial H/\partial \mathbf{x} = -\lambda^T(\partial \mathbf{f}/\partial \mathbf{x}) \tag{4.5.6}$$

so that

$$\dot{\lambda}_E = -\lambda_E(\partial f_1/\partial E) - \lambda_h(\partial f_2/\partial E) - \lambda_g(\partial f_3/\partial E) - \lambda_W(\partial f_4/\partial E) - \lambda_Q(\partial f_5/\partial E)$$
$$\dot{\lambda}_h = -\lambda_E(\partial f_1/\partial h) - \lambda_h(\partial f_2/\partial h) - \lambda_g(\partial f_3/\partial h) - \lambda_W(\partial f_4/\partial h) - \lambda_Q(\partial f_5/\partial h)$$

etc....

Note that the equations of motion contain terms involving quantities such as V, L, D, R, and T that are functions of the states. Thus, to fully express the required derivatives of $\mathbf{f}$, it is necessary either to express these quantities in terms of the states before differentiating or to differentiate the quantities with respect to the states and use the chain rule. The control equation is

$$0 = \partial H/\partial u = \partial H/\partial \alpha = \lambda^T \partial \mathbf{f}/\partial \alpha$$
$$= -\lambda_E \partial f_1/\partial \alpha - \lambda_h \partial f_2/\partial \alpha - \lambda_g \partial f_3/\partial \alpha - \lambda_W \partial f_4/\partial \alpha - \lambda_Q \partial f_5/\partial \alpha \tag{4.5.7}$$

Because the first two equations of motion contain L and D, which are functions of $\alpha$, the above remark for the adjoint equations applies here.

To derive the transversality conditions, note that there are 11 unknowns (5 states + 5 adjoints + $t_f$) and 8 boundary conditions. Thus, 3 new boundary conditions are expected from transversality. They are:

$$0 = \partial G/\partial \mathbf{x}(t_f) + (\partial F/\partial \dot{\mathbf{x}})_{t_f} = \partial G/\partial \mathbf{x}(t_f) + \lambda^T(t_f)$$
$$\Rightarrow \lambda_\gamma(t_f) = 0, \lambda_W(t_f) = -1 \tag{4.5.8}$$

$$0 = \partial G/\partial t_f + (F - (\partial F/\partial \dot{\mathbf{x}})\dot{\mathbf{x}})\,|_{t_f} = \partial G/\partial t_f + H\,|_{t_f}$$
$$\Rightarrow H\,|_{t_f} = 0 \tag{4.5.9}$$

In light of the development given in this section, the trajectory optimization problem can be restated as follows: solve the 5 state variables, 5 adjoints, 1 control, and $t_f$ that will satisfy the 5 state equations, 5 adjoint equations, control equation, and 11 boundary conditions. This two-point boundary value problem may be solved, for example, by the "shooting" method. The method itself is described in Appendix A, while the application of the shooting method to this particular problem is detailed in Appendix B.

## V. RESULTS OF BASELINE OPTIMAL TRAJECTORY

For the baseline vehicle, with heat load unconstrained, total flight time was 238.8 sec., final slant range was 3.183 x $10^6$ ft., and final weight fraction was .5890 (i.e., 123,300 lb of fuel expended). Time histories of the states and adjoints are given in Figures 5 and 6. All states are shown in the nondimensional form defined earlier except altitude, which is plotted in dimensional form for convenience. Note also that it is expressed as $h - h_0$, again because the orbit injection maneuver will begin at some nonzero altitude.

The value of $C_Q$ for the unconstrained heating solution was found to be approximately 142, corresponding to a total heat soak of 5.291 x $10^5$ BTU/ft$^2$. Thus setting $C_Q$ at 142 yielded a solution for which $\lambda_Q$ was of the order $10^{-7}$, very near the necessary value of zero.

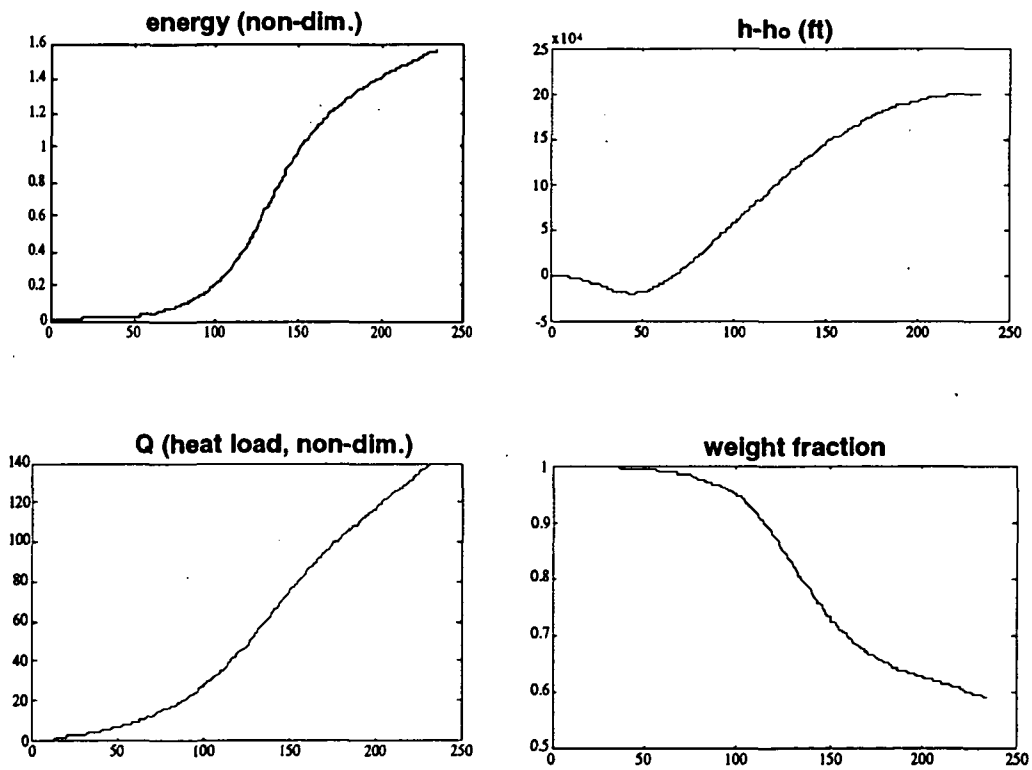


Fig. 5. State Histories.

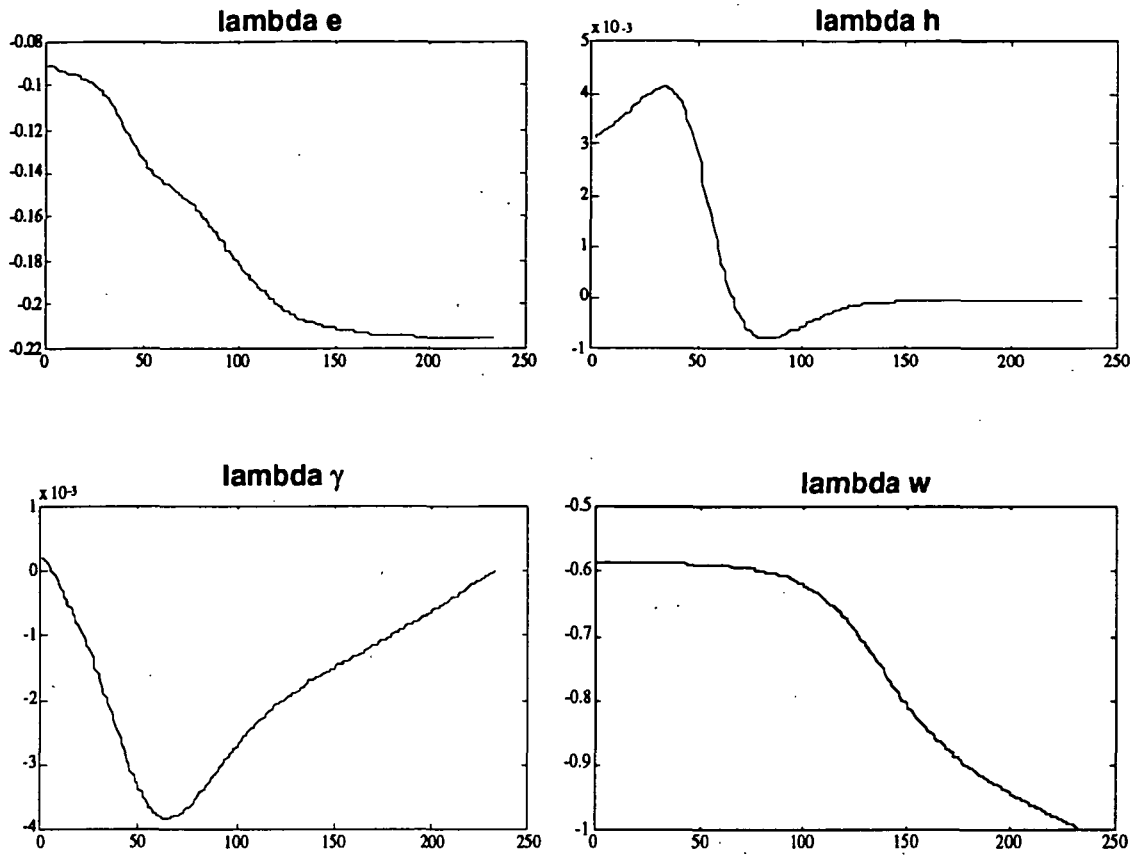


Fig. 6. Adjoint Time Histories.

Velocity and dynamic pressure are plotted in Figure 7. It is evident that before climbing, the vehicle must dive down below the initial altitude to a higher dynamic pressure in order to trade potential for kinetic energy and thus attain a more desirable flight condition. It is then able to ascend rapidly before levelling off slightly at the point of orbit injection. Peak dynamic pressure is approximately 9000 psf, which is much higher than the 1500 to 2000 anticipated for NASP [9].

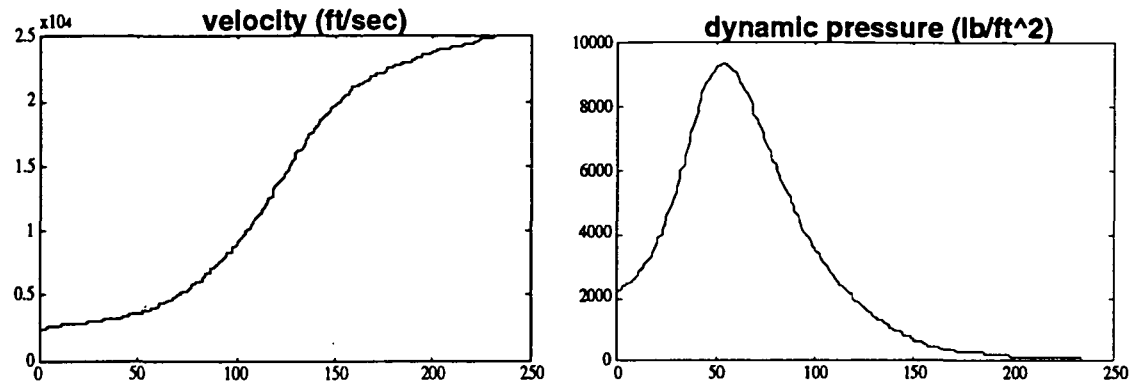


Fig. 7. Velocity and Dynamic Pressure Histories.

Lift and flight path angle are plotted together in Figure 8, while drag, thrust, and fuel flow are plotted in Figure 9. (Note that lift, drag, and thrust are shown in the non-dimensional form defined earlier.) As expected, fuel flow rate is seen to increase with acceleration (i.e., thrust minus drag). Maximum fuel flow is extremely high (approximately 1600 lb/sec) compared to reasonable values for other classes of vehicles. Thrust turns out to be a very large quantity as well, peaking at approximately 2.1 x $10^6$ lb.

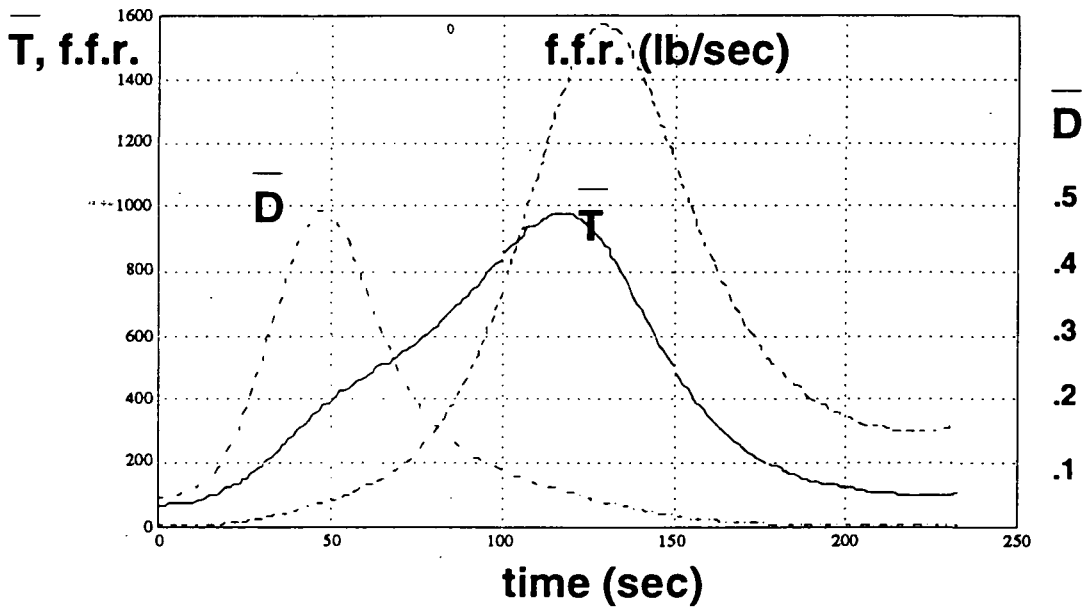


Fig. 8. Thrust, Drag, and Fuel Flow Histories.

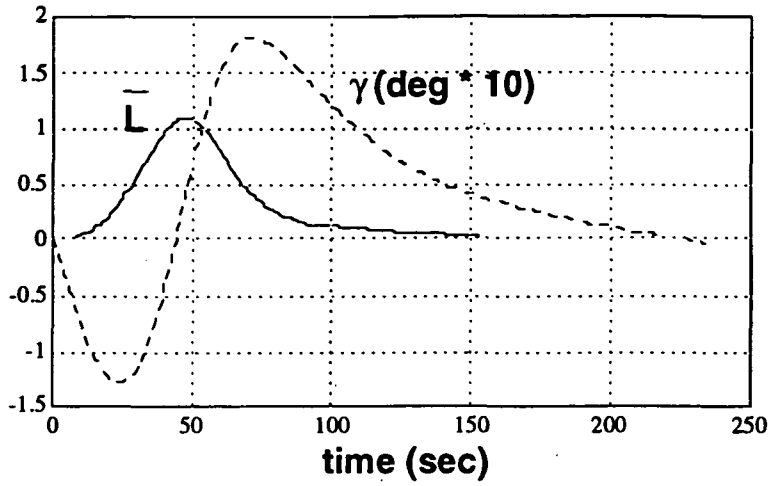


Fig. 9. Lift and Flight Path Angle.

To examine the effect of imposing a heating constraint, solutions were obtained for various values of $C_Q$ less than 140, and the resulting trajectories were investigated. Figures 10 and 11 show both the unconstrained trajectory and a trajectory for which the final heat load was constrained to approximately half that of the unconstrained (approximately 2.4 x $10^5$ BTU/$ft^2$). Figure 10 also shows contours of constant energy E, dynamic pressure q, and heat-transfer rate $\dot{Q}$. Each of the two figures shows the trajectories indexed with time. Flight time for the constrained case is reduced significantly to 84.0 sec, and final orbital mass fraction is .5864 (124,080 lb of fuel expended), a decrease of only about .4 % from the unconstrained result. Compared to the unconstrained trajectory, the trajectory with the heat-load constraint descends lower, to a greater dynamic pressure, and gains more kinetic energy before beginning its ascent. Note also that from approximately Mach 8 to Mach 17, the constrained trajectory follows a path of almost constant dynamic pressure at 10,000 psf. An interesting result is that the constrained optimal trajectory experiences much higher heating rates, but the trajectory duration is less than half that for the unconstrained trajectory, thus halving the total heat load.

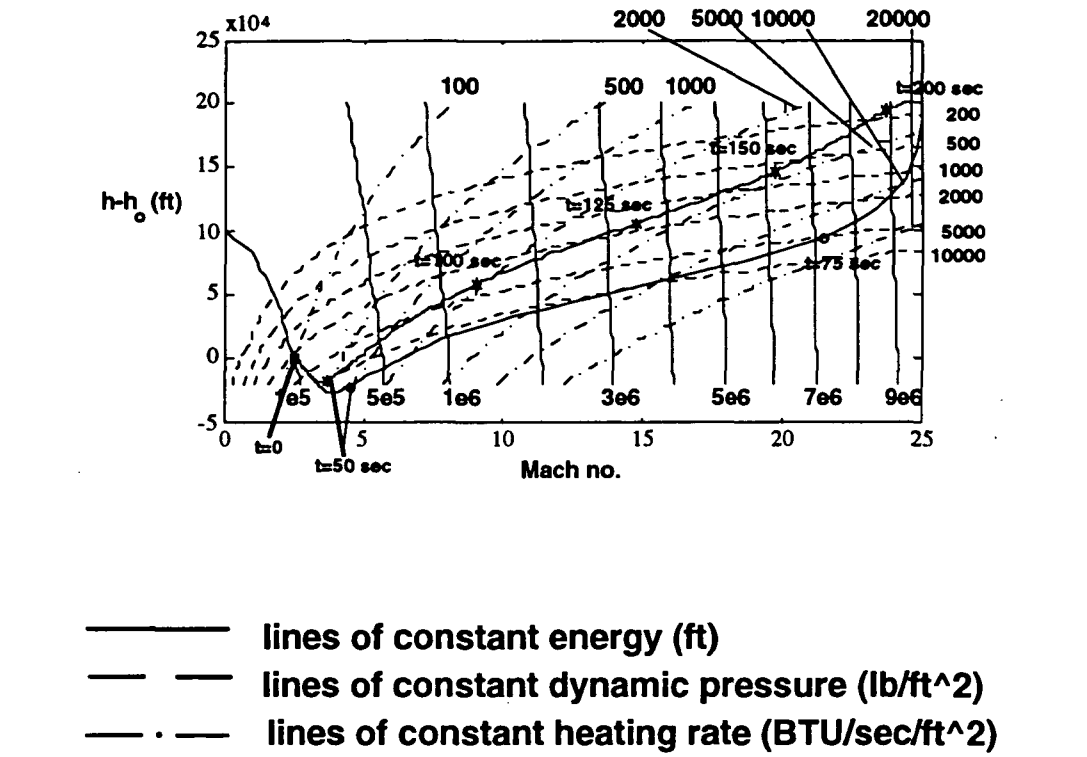


Fig. 10. Vehicle Trajectory--Altitude vs. Mach number.

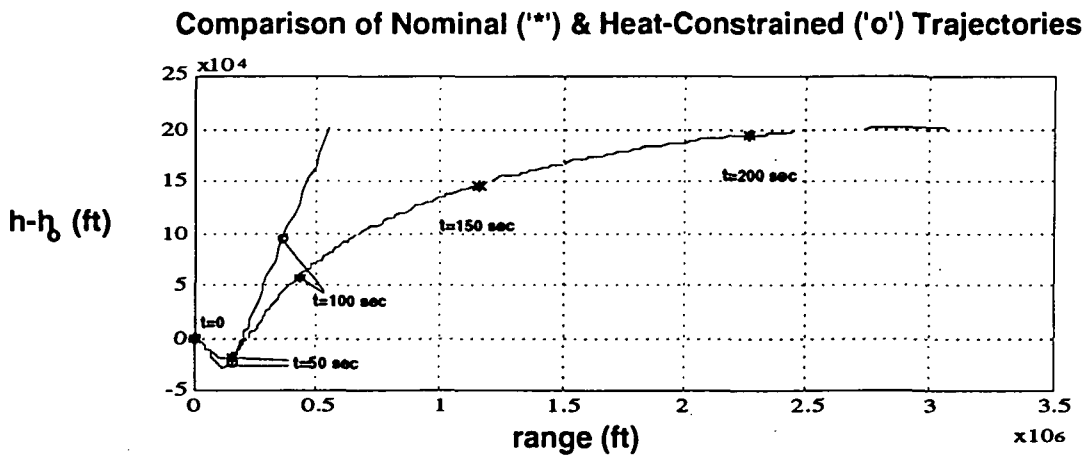


Fig. 11. Vehicle Trajectory--Altitude vs. Range.

## VI. SUBSYSTEM MISSION PERFORMANCE SENSITIVITIES

For each vehicle configuration described in Chapter 3, the maximum orbital mass fraction was determined by solving numerically for the minimum-fuel trajectory. This was done using the shooting method (Appendix A) and following the procedure in Appendix B. Table 2 lists the key parametric results. Shown in this table are not only the maximum orbital mass fractions for each configuration, but also the mission flight time to achieve orbital energy, the final slant range when orbital energy is achieved, and the total heating load experienced by the vehicle over the entire trajectory. Also shown for each configuration are the same results for an optimal trajectory that is constrained to yield a fixed value of total heat soak. For the puposes of this analysis, a heating constraint of $2.48 \times 10^5$ BTU/ft$^2$ was placed on all configurations. The heating constraint is a means of effectively decreasing the vehicle's structural efficiency. Thus the tabulated results below illustrate the effects of four different subsytem efficiencies on mission performance.

**Table 2 - Final Values of Time, Range, Total Heat Soak, and Total Weight Fraction for Each Model (For Unconstrained and Constrained Heating)**

| | $t_f$(sec) | | Range (ft) | | $Q_f$(BTU/ft^2) | | $W_f/W_o$ | |
|---|---|---|---|---|---|---|---|---|
| Model | unconst. | constr. | unconst. | constr. | unconst. | constr. | unconst. | constr. |
| Baseline | 238.8 | 103.9 | 3.183e6 | 7.927e5 | 5.29e5 | 2.48e5 | .5890 | .5872 |
| High L/D | 222.1 | 98.5 | 2.905e6 | 7.985e5 | 5.10e5 | 2.48e5 | .5962 | .5947 |
| High T/W | 230.3 | 107.4 | 3.038e6 | 8.585e5 | 4.95e5 | 2.48e5 | .5901 | .5886 |
| Low SFC | 234.0 | 102.3 | 3.079e6 | 7.753e5 | 5.30e5 | 2.48e5 | .6211 | .6194 |

The trajectories corresponding to the baseline configuration were discussed previously. The trajectories for the remaining cases are similar. For unconstrained heating, all the high-efficiency configurations achieve orbit with higher weight fraction than the baseline, as expected from equation (3.4). Moreover, the high-efficiency configurations all complete the mission faster than the baseline. As a result of the imposed heating constraint, the mission time for each configuration decreases

drastically from its unconstrained value, while the penalty in orbital mass fraction is small--about .3% less payload for each configuration.

Now consider the mission performance, i.e., the weight placed into orbit, expressed in terms of the subsystem sensitivities $S_1$-$S_4$ by the following equation:

$$\Delta \text{ Orbital Weight} = (S_1)\,\Delta(L/D)_o + (S_2)\,\Delta(T/W)_o + (S_3)\,\Delta(\text{s.f.c.})_o + (S_4)\,\Delta Q_{final}$$

Each sensitivity $S_i$ is defined as the change in payload to orbit divided by the percent increase in the efficiency of one subsystem while holding the other subsystem efficiencies constant, i.e., at their baseline values. The $\Delta$ terms above represent the percent change from baseline values in $(L/D)_o$, $(T/W)_o$, $(\text{s.f.c.})_o$, and $Q_{final}$, respectively. Of course, an increase in orbital weight leads directly to a corresponding increase in payload to orbit, if the structural mass fraction is constant and all fuel is expended. From the results in Table 2 and the subsystem efficiency increases presented in Chapter 3, assuming a gross takeoff weight of 300,000 lb, the numerical values for the subsystem sensitivities $S_1$-$S_4$ for the unconstrained heating case are

$S_1$ = 30 lb / (% increase in $(L/D)_o$)

$S_2$ = 24 lb / (% increase in $(T/W)_o$)

$S_3$ = 954 lb / (% decrease in $(\text{s.f.c.})_o$)

$S_4$ = 12 lb / (% increase in $Q_{final}$)

If the total heat load is constrained, the subsystem efficiencies change. In this case, $S_4$ is not applicable, and the other three sensitivities become

$S_1$ = 33 lb payload / (% increase in $(L/D)_o$)

$S_2$ = 36 lb payload / (% increase in $(T/W)_o$)

$S_3$ = 966 lb payload / (% decrease in $(\text{s.f.c.})_o$)

Note that, while the magnitudes of $S_1$ and $S_3$ remain about the same as for the unconstrained case, $S_2$ has increased significantly. Thus, based on this method of

representing subystem senstivities, T/W appears to have a larger influence on mission performance when the heating load is constrained. The above results are summarized graphically in the carpet plot of Figure 12. This figure shows the variation in orbital mass fraction due to variations in $(s.f.c.)_o$, $(T/W)_o$, and $(L/D)_o$. In the case of both constrained and unconstrained heating, the lower left corner of the plot represents the baseline values.

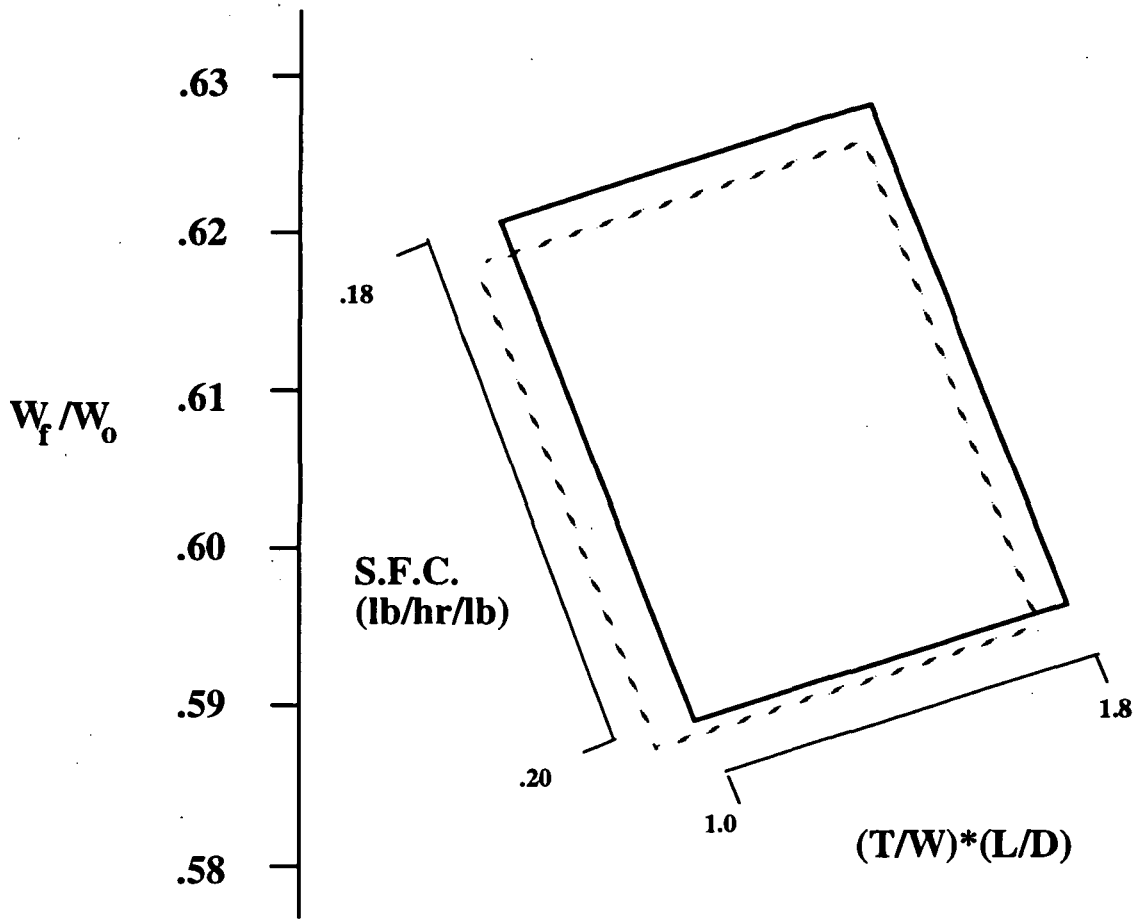


Fig. 12. Mission Performance Sensitivities for Unconstrained (_____) and Constrained (- - - -) Heating.

Consider again equation (3.4). If $(s.f.c.)_o$, $(T/W)_o$, and $(L/D)_o$ are known, this equation makes it possible to calculate approximately $dE/dW_f$ at the takeoff condition, or $(dE/dW_f)_o$. However, the values of s.f.c., T/W, and L/D--and therefore $dE/dW_f$--vary widely throughout the trajectory. This suggests that it would be useful to examine the average values of L/D, T/W, and s.f.c. over the entire trajectory for each

configuration. Each sensitivity above is calculated by evaluating the performance at a single condition (the nominal "takeoff" condition) and comparing it to baseline performance. Recall from Table 1 that for each configuration, this resulted in a higher value of one efficiency parameter evaluated at the "takeoff" condition, while the other parameters remained constant. For example, for the high-(L/D) configuration, this resulted in $(L/D)_o$ above the baseline value, and the same $(T/W)_o$ and $(s.f.c.)_o$ as the baseline. However, due to the high degree of coupling in the problem, $(T/W)_{avg}$ and $(s.f.c.)_{avg}$ will generally *not* be the same as for the baseline case. This is due in part to the fact that decreasing the drag coefficient changes the optimal value of $\alpha$. And as $\alpha$ feeds back into the equations of motion, it affects (T/W) and (L/D) as well. In other words, an increase in one subsystem efficiency will have some effect on other subsystem efficiencies over the course of the trajectory. This is borne out in the following tabular data. Table 3 displays $(L/D)_{avg}$, $(T/W)_{avg}$, and $(s.f.c.)_{avg}$ for each configuration, along with the average value of the parameter $dE/dW_f$ as computed by equation (3.4). Table 4 displays these results for the heat-constrained case.

**Table 3 - Subsystem Performance Comparison for Each Model (UNCONSTRAINED case)**

| Model | $(L/D)_{avg}$ | $(T/W)_{avg}$ | $(SFC)_{avg}$ (lb/hr/lb) | $(dE/dW_f)_{avg}$ |
|---|---|---|---|---|
| Baseline | 1.689 | 5.108 | 3.147 | .019227 |
| High L/D | 5.732 | 5.099 | 3.184 | .02090 |
| High T/W | 1.698 | 5.128 | 3.153 | .019231 |
| Low SFC | 1.690 | 5.185 | 2.852 | .02105 |

**Table 4 - Subsystem Performance Comparison (CONSTRAINED case)**

| Model | $(L/D)_{avg}$ | $(T/W)_{avg}$ | $(SFC)_{avg}$ (lb/hr/lb) | $(dE/dW_f)_{avg}$ |
|---|---|---|---|---|
| Baseline | 1.754 | 22.943 | 3.168 | .02118 |
| High L/D | 5.488 | 21.827 | 3.195 | .02139 |
| High T/W | 1.749 | 20.195 | 3.167 | .02122 |
| Low SFC | 1.759 | 23.821 | 2.867 | .02311 |

Note that both with and without the heating constraint, $(L/D)_{avg}$ increases significantly for the high-$(L/D)_o$ configuration, and similarly the average specific fuel consumption decreases for the low-$(s.f.c.)_o$ configuration. However, the analogous situation does not occur for the high-$(T/W)_o$ model. Indeed, $(T/W)_{avg}$ increases only slightly for this configuration in the unconstrained case, and decreases in the constrained case. This type of result would not be expected for a vehicle with less dynamic coupling.

Due to the approximate nature of equation (3.4), the vehicle configurations for the heat-constrained case display larger average values of $dE/dW_f$ than those for the unconstrained case. Still, the trends exhibited by the four configurations in each case are clear. Consider an alternate set of subsystem sensitivites, defined as follows:

$$\Delta (dE/dW_f)_{avg} = (\bar{S}_1)\, \Delta(L/D)_o + (\bar{S}_2)\, \Delta(T/W)_o + (\bar{S}_3)\, \Delta(s.f.c.)_o$$

where

$$\bar{S}_1 = .133(\%\text{ increase in } (dE/dW_f)_{avg}) \,/\, (\%\text{ increase in } (L/D)_o)$$

$$\bar{S}_2 = .0208(\%\text{ decrease in } (dE/dW_f)_{avg}) \,/\, (\%\text{ increase in } (T/W)_o)$$

$$\bar{S}_3 = .948(\%\text{ decrease in } (dE/dW_f)_{avg}) \,/\, (\%\text{ decrease in } (s.f.c.)_o)$$

for no heating constraint, and

$\bar{S}_1$ = .0144(% increase in $(dE/dW_f)_{avg}$) / (% increase in $(L/D)_o$)

$\bar{S}_2$ = .0189(% decrease in $(dE/dW_f)_{avg}$) / (% increase in $(T/W)_o$)

$\bar{S}_3$ = .911(% decrease in $(dE/dW_f)_{avg}$) / (% decrease in $(s.f.c.)_o$)

with heating constraint. Again, due to simplifications in the derivation of equation (3.4), the computed values of $(dE/dW_f)_{avg}$ in Tables 3 and 4 are approximate. However, the general trends for the $\bar{S}_i$'s are in line with those of the $S_i$'s defined previously--specifically, the sensitivity $\bar{S}_3$ is much larger than $\bar{S}_1$ or $\bar{S}_2$ both with and without heating constraint. Thus the data in Tables 3 and 4 offers some insight as to the effect that a change in one subsystem efficiency has on the overall system efficiency, as well as on the other subsystem performance parameters, over the entire trajectory. Both sets of sensitivities defined in this section suggest that, from a vehicle designer's perspective, vehicle fuel efficiency is the most critical design aspect with regard to its effect on overall system efficiency. As stated in Section 3, maximum overall system efficiency translates directly into maximum mission performance, i.e., maximum payload to orbit.

# VII. CONCLUSIONS

Single-stage-to-orbit (SSTO) vehicles have unique characteristics. Like an aircraft, they rely on significant aerodynamic lift and have smaller thrust-to-weight ratios than rockets. But like rockets, their mission is to maximize payload into orbit, and propulsive and structural efficiencies are extremely important. The orbit-insertion mission here is more one of climbing in the atmosphere than cruising like an aircraft or a ballistic launch. But the sizing of SSTO vehicles leads to a unique problem. The sizing problem has been formulated for a generic hypersonic vehicle model utilizing an optimization paradigm, built around minimum-fuel optimal trajectories, and defining mission performance in terms of the maximum amount of payload placed into orbit. The optimal trajectory involves a zoom/climb, reminiscent of classical aircraft climb performance. Although orbital mass fraction for the mission is approximately 60% for all the configurations considered here, results indicate that this value is a strong function of L/D and s.f.c., and depends on the T/W ratio as well. In addition, a heating model has been incorporated into the problem as a means of constraining the heat load experienced by the vehicle. Although a heating constraint clearly can reduce the maximum orbital mass fraction for a given vehicle, trajectory shaping via optimization can significantly reduce this deleterious effect.

## VIII. REFERENCES

1. Aviation Week and Space Technology, Oct. 29, 1990, p. 46.

2. Lovell, T.A., Schmidt, D.K., and Chavez, F.R., "Minimum-fuel Trajectories for Hypersonic Vehicles with Aeropropulsive Interactions," AIAA Paper 93-3660, Atm. Flight Mech. Conf., Monterey, CA, August, 1993.

3. Bilimoria, K.D., and Schmidt, D.K., "An Integrated Development of the Equations of Motion for Elastic Hypersonic Flight Vehicles," technical report ARC92-3, prepered by the Aerospace Research Center, ASU, for NASA Langley Research Center, July, 1992.

4. Schmidt, D. K. and Chavez, F.R., "An Integrated Analytical Aeropropulsive/Aeroelastic Model for the Dynamic Analysis of Hypersonic Vehicles," AIAA Paper 92-4567, Atm. Flight Mech. Conf., August, 1992.

5. Chavez, F.R. and Schmidt, D.K., "Dynamics of Hypersonic Flight Vehicles Exhibiting Significant Aeroelastic and Aeropropulsive Interactions," AIAA Guidance, Navigation, and Control Conf., Monterey, CA, August, 1993.

6. Shaughnessy, J.D., Pinckney, S.Z., and McMinn, J.D., "Hypersonic Vehicle Simulation Model: Winged-Cone Configuration," NASA Technical Memorandum 102610, November 1990. 91N12705

7. Bossard, J.A., Peck, R.E., and Schmidt, D.K., "An Extended Supersonic Combustion Model for the Dynamic Analysis of Hypersonic Vehicles," Technical report ARC93-2, prepared by the Aerospace Research Center, ASU, for NASA Langley Res. Center, March, 1993.

8. Martin, John J., Atmospheric Entry, Prentice-Hall, 1966.

9. Schmidt, D. K., Mamich, H., and Chavez, F., "Dynamics and Control of Hypersonic Vehicles - The Integration Challenge for the 1990's," AIAA Paper 91-5057, Dec., 1991.

# A. NUMERICAL SOLUTION METHOD

## A.1 Shooting Method

The shooting method for solving two-point boundary value problems involves guessing the unspecified initial conditions, integrating forward, and updating the guesses (via a Newton-Raphson routine) based on the error between the actual and desired terminal conditions. The method as applied to this particular problem proceeds as follows:

Define the states and adjoints together as $\mathbf{X} = [\mathbf{X}_1\ \mathbf{X}_2]^T$, where $\mathbf{X}_1 = [E\ h\ \gamma\ W\ Q]^T$ are the elements of $\mathbf{X}$ that are specified at the initial time and $\mathbf{X}_2 = [\lambda_E\ \lambda_h\ \lambda\gamma\ \lambda_W\ \lambda_Q]^T$ are the elements of $\mathbf{X}$ that are unspecified at the initial time. (Note that for this problem $\mathbf{X}_1$ is comprised entirely of states and $\mathbf{X}_2$ entirely of adjoints, although generally this may not be the case.) Thus the state and adjoint equations can be written as

$$\dot{\mathbf{X}} = \mathbf{F}, \quad \text{where } \mathbf{F} = [\mathbf{f}\ \ -\partial H/\partial \mathbf{x}]^T \tag{A.1.1}$$

Define $\mathbf{M}(t) = \partial \mathbf{X}(t)/\partial \mathbf{X}_2(t_o)$. From this we see that

$$\mathbf{M}(t_o) = \partial \mathbf{X}(t_o)/\partial \mathbf{X}_2(t_o) = [\mathbf{0}\ \ \mathbf{I}_5]^T \tag{A.1.2}$$

and

$$\dot{\mathbf{M}} = \partial \dot{\mathbf{X}}(t)/\partial \mathbf{X}_2(t_o) = \partial \mathbf{F}/\partial \mathbf{X}_2(t_o) = \partial \mathbf{F}/\partial \mathbf{X}(t) * \partial \dot{\mathbf{X}}(t)/\partial \mathbf{X}_2(t_o) = \partial \mathbf{F}/\partial \mathbf{X}(t) * \mathbf{M} \tag{A.1.3}$$

With the initial condition on $\mathbf{M}$ (4.1.2), Equation (4.1.3) can be integrated together with (4.1.1) at each time step. Now define

$$\Psi_m(t) = [E(t)-E_f,\ h(t)-h_f,\ \lambda\gamma(t)-\lambda\gamma_f,\ \lambda_W(t)-\lambda_{Wf},\ H(t)-H_f]^T \tag{A.1.4}$$

where $E_f$, $h_f$, etc., are the final conditions specified for the states, adjoints, and Hamiltonian. So

$$\Psi_m(t_f) = [E(t_f)-E_f,\ h(t_f)-h_f,\ \lambda\gamma(t_f), \lambda_W(t_f)+1, H(t_f)]^T \qquad (A.1.5)$$

Note that

$$\partial\Psi_m(t_f)/\partial\mathbf{X}_2(t_o) = \partial\Psi_m(t_f)/\partial\mathbf{X}(t_f)*\partial\mathbf{X}(t_f)/\partial\mathbf{X}_2(t_o) = \partial\Psi_m(t_f)/\partial\mathbf{X}(t_f)*\mathbf{M}(t_f) \qquad (A.1.6)$$

After (A.1.1) and (A.1.3) are integrated up to $t_f$, $\mathbf{M}(t_f)$ is known and $\partial\Psi_m(t_f)/\partial\mathbf{X}(t_f)$ can be calculated. Thus $\partial\Psi_m(t_f)/\partial\mathbf{X}_2(t_o)$, a 5x5 matrix, is known.

To solve for $\mathbf{X}_2(t_o)$ (which for this problem consists of the initial adjoints $\lambda(t_o)$) that will drive $\Psi_m(t_f)$ to its desired value of [**0**], an initial guess for $\mathbf{X}_2(t_o)$ is made and the state equations for **X** and **M** are integrated from $t_o$ to $t_f$. The Taylor series expansion of $\Psi_m(t_f)$ as a function of $\mathbf{X}_2(t_o)$ gives

$$\Psi_m(t_f)_{i+1} = \Psi_m(t_f)_i + (\partial\Psi_m(t_f)/\partial\mathbf{X}_2(t_o))_i * \Delta\mathbf{X}_2(t_o)_i \qquad (A.1.7)$$

where the desired value of $\Psi_m(t_f)_{i+1}$ is [**0**], $\Psi_m(t_f)_i$ and $(\partial\Psi_m(t_f)/\partial\mathbf{X}_2(t_o))_i$ are computed from the integration, and $\Delta\mathbf{X}_2(t_o)_i$ gives the amount by which to increment $\mathbf{X}_2(t_o)$ in order to reach the desired $\Psi_m(t_f)$. So the initial guess for $\mathbf{X}_2(t_o)$ is updated according to

$$\mathbf{X}_2(t_o)_{i+1} = \mathbf{X}_2(t_o)_i + \Delta\mathbf{X}_2(t_o)_i$$

$$= \mathbf{X}_2(t_o)_i + (\partial\Psi_m(t_f)/\partial\mathbf{X}_2(t_o))^{-1}(\Psi_m(t_f)_{desired} - \Psi_m(t_f)_i)$$

$$= \mathbf{X}_2(t_o)_i - (\partial\Psi_m(t_f)/\partial\mathbf{X}_2(t_o))^{-1}\Psi_m(t_f)_i \qquad (A.1.8)$$

Because changes in $\Psi_m(t_f)$ can be very sensitive to changes in $\mathbf{X}_2(t_o)$, this equation is modified by

$$\mathbf{X}_2(t_o)_{i+1} = \mathbf{X}_2(t_o)_i - \sigma(\partial\Psi_m(t_f)/\partial\mathbf{X}_2(t_o))^{-1}\Psi_m(t_f)_i \qquad (A.1.9)$$

where $\sigma$ is a step size parameter between 0 and 1. Use the updated $\mathbf{X}_2(t_o)$ to integrate again from $t_o$ to $t_f$. Iterating in this manner will cause $\mathbf{X}_2(t_o)$ to converge to $\mathbf{X}_2^*(t_o)$ corresponding to the optimal solution. There are a number of possible critieria to determine convergence, such as $\|\Psi_m(t_f)_i\| < \varepsilon$ or $\|\mathbf{X}_2(t_o)_{i+1} - \mathbf{X}_2(t_o)_i\| < \varepsilon$.

Two issues still to be addressed are determination of $t_f$ and determination of the optimal control $\alpha_{opt}$.

## A.2 Determination of $t_f$

Six boundary conditions have been specified or derived at the final time. Five of them are used in the definition of $\Psi_m(t)$ in order to determine the five initial adjoints $\mathbf{X}_2(t_o)$ via Equation (A.1.9). The sixth, $Q(t_f) = C_Q$, is used as a stopping condition (i.e., the terminal time $t_f$ has been reached when the value of Q reaches $C_Q$). Any of the final conditions can be used for this purpose. However, as can be seen from the fifth EOM, Q always increases monotonically from zero. This guarantees that the value of Q will reach $C_Q$ at some point and will reach it only once, making it a good candidate for a stopping condition.

This raises the question of how to choose $C_Q$. Different minimum-fuel trajectories can be achieved for various choices of $C_Q$, each representing a certain degree of heating constraint. Initially, it is desired to find the minimum-fuel trajectory with no heating constraint. From the derivation of the Euler-LaGrange adjoint equations, it is readily seen that $\lambda_Q = 0$. That is, because **f** is not a function of Q, the quantity $\lambda^T(\partial \mathbf{f}/\partial Q)$ is zero. Therefore, $\lambda_Q$ is constant throughout the trajectory. Since $\lambda_Q$ indicates the sensitivity of J to changes in Q, the "unconstrained heating solution" will be the minimum-fuel trajectory corresponding to $\lambda_Q = 0$. Of course, the value of $C_Q$ that will yield this solution is not known *a priori*. Yet, as long as a solution can be obtained for some arbitrary value of $C_Q$, it is likely that the unconstrained heating solution can be found by repeatedly perturbing $C_Q$ and recomputing a solution until $\lambda_Q$ is near zero to within some tolerance. Once the unconstrained solution is obtained, $C_Q$ can then be varied to yield heat-constrained solutions.

## A.3 Determination of $\alpha_{opt}$

The optimal control, which satisfies the control equation $\partial H/\partial\alpha=0$ (2.5.9), is determined at each time step by the Newton iteration formula

$$\alpha_{i+1} = \alpha_i - [(\partial H/\partial\alpha)/(\partial^2 H/\partial\alpha^2)]_{\alpha=\alpha_i} \qquad (A.3.1)$$

The initial guess for $\alpha_{opt}$ is 1° at $t=t_o$ and thereafter is the previous value of $\alpha_{opt}$. There are a number of possible critieria to determine convergence, such as $\|\partial H/\partial\alpha\| < \varepsilon$ or $\|\alpha_{i+1} - \alpha_i\| < \varepsilon$.

## B. SOLUTION PROCEDURE

### B.1 Baseline Configuration

Due to the tight coupling and nonlinearities inherent in the state equations, solution of the full mission trajectory by the above method tends to require extremely accurate guesses of the initial adjoints $\lambda(t_o)$. In addition, because the adjoints are contrived parameters and not physical quantities, it is difficult to determine what the magnitude of these parameters should be. The problem was solved by means of an extrapolation or "bootstrapping" procedure, which is described as follows:

**1)**Pick an "intermediate" trajectory, i.e., one that begins at the initial flight condition given in Chapter 2, but terminates at an altitude and velocity much lower than orbital values. An estimate of the value of $C_Q$ (the specified terminal condition on Q) for this trajectory is obtained by guessing $\lambda(t_o)$, integrating forward from the initial state until one of the specified terminal values (such as altitude or velocity) is reached, and noting the final value of Q. For several different guesses of $\lambda(t_o)$, the values of $Q(t_f)$--and the other final state values--give an indication as to the size of $C_Q$ required. The numerical solution method of the previous section is then applied to the intermediate trajectory. (Note that in picking an intermediate trajectory, the final conditions on E, h, and Q are different from their values for the full trajectory. However, by transversality, the conditions on $\lambda_\gamma(t_f)$, $\lambda_W(t_f)$, and $H(t_f)$ remain the same.)

**2)**Once $\lambda(t_o)$ corresponding to the optimal solution (call this $\lambda^*(t_o)$ ) is found for this short trajectory, the next step is to obtain a solution for a longer trajectory (i.e., a higher energy level) by extrapolation. One method of extrapolating from one trajectory to the next is to begin with the current $\lambda^*(t_o)$ and integrate past the terminal conditions of the current trajectory to a higher energy level. The values of E, h, and $C_Q$ at this energy level become the new $E_f$, $h_f$, and $C_Q$, and the current $\lambda^*(t_o)$ becomes the initial guess of $\lambda(t_o)$ for the new trajectory. The numerical solution method is then applied to the new trajectory.

**3)**As this process continues, the specified terminal conditions for each intermediate trajectory are made to approach those for the full (desired) trajectory until a solution for the full orbit injection mission trajectory is reached.

As the above solution procedure was followed, it was found that for each intermediate trajectory, the smaller the change in energy level from the previous trajectory, the faster the solution method converged. It should also be noted that the minimum-fuel solution for each intermediate trajectory need not be the one corresponding to unconstrained heating load for that trajectory. At each intermediate step, finding a minimum-fuel solution for *some* value of $C_Q$--not necessarily the one for unconstrained heating--made it possible to march toward the final trajectory by extrapolation. Only in the case of the final trajectory is the particular value of $C_Q$ of importance.

B.2 High Efficiency Configurations

In solving the minimum fuel trajectory for each high efficiency configuration, the full trajectory solution for the baseline model was used as a "starting" solution. The general procedure is here described for the low-s.f.c. configuration: The engine constant $C_3$ was first decreased by approximately 1%. Using $\lambda^*(t_o)$ for the baseline trajectory as the initial guess for $\lambda(t_o)$, a convergent solution was obtained for the perturbed configuration by the shooting method. Then, using the current values of $\lambda^*(t_o)$ as an initial guess for $\lambda(t_o)$, a solution was obtained for $C_3$ decreased slightly further. This process continued, perturbing $C_3$ a little at a time and re-optimizing, until the constant was 10% below its baseline value. Similarly, in the case of the high T/W configuration, the engine constants $C_1$ and $C_2$ were increased slowly from their baseline values until they were 10% higher; and for the high L/D model, the $C_{D_o}$ was decreased slowly from its baseline value to zero.